Bull. Mater. Sci. (2020) 43:134
https://doi.org/10.1007/s12034-020-02104-8

Influence of incorporation of carbon on the transparent conducting properties of CdO thin films

A A DAKHEL
Department of Physics, College of Science, University of Bahrain, P.O. Box 32038, Zallaq, Kingdom of Bahrain
adakhil@uob.edu.bh

MS received 20 February 2019; accepted 28 October 2019

Abstract. Thin films of CdO incorporated with different amounts of carbon element have been deposited on glass substrates by using the vacuum thermal evaporation method aiming at improving their transparent conducting (TC) properties. The structural and opto-electrical properties of the host CdO films were systematically studied. X-ray diffraction and optical investigations confirmed the inclusion of C species in the CdO lattice. The obtained results were explained through the occupation of interstitial positions and structural vacancies of the host CdO lattice by C species. It was observed that the inclusion of carbon into the CdO lattice blue-shifted the optical band gap by ∼5−7%, which was attributed to the Moss–Burstein (B–M) effect. The electrical studies showed that the carrier mobility increased steadily with the increase in the C% inclusion level, so that with 5 wt% it attained ∼7.5 times the carrier mobility in un-doped CdO. Therefore, the present study showed that the prepared host CdO–C films have controllable TC degenerate semiconducting properties, which could be required in different optoelectronic applications.

Keywords. Cadmium–carbon oxide; C-incorporated CdO films; CdO films.

1. Introduction

Group of transparent conducting oxides (TCOs) such as ZnO, CdO, In_2O_3 and SnO_2 have manifold applications in the field of optoelectronics such as manufacturing of solar cells, phototransistors and flat panels, and in other fields such as gas-sensing applications [1–3]. Pristine TCOs have degenerate semiconducting n-type properties with relatively low resistivity. Their opto-conducting properties are attributed to natural point defects such as oxygen vacancies and metal interstitials.

CdO films are transparent, especially in the near-infrared (NIR) spectral region, as their band gap is in the range of 2.2–2.7 eV, with a low resistivity of $10^{-2} - 10^{-3}\ \Omega$ cm [1,3,4]. The optoelectronic properties of TCOs, including CdO can be controlled by adjusting its point defects. The superior method to develop the transparent conducting (TC) function of CdO is by improving its conduction parameters, CPs (conductivity (σ), carrier mobility (μ) and optical transparency), especially μ rather than increasing N_{el}, because an increase in N_{el} causes reduction in the optical transparency of the film. Therefore, the fabrication of TCO CdO is considered as a compromise between high conductivity and low absorbance. The usual method used to improve the CPs is by doping/inclusion of exotic ions. It was observed experimentally that the size and valency of dopant/incorporated ions have great influence on the properties of the prepared host CdO. Consequently, the CPs of CdO were improved by doping with ions of slightly smaller volume than that of Cd^{2+} ions (0.095 nm [5]). However, when focusing on carrier mobility, it was observed that the mobility was significantly improved by doping with small-sized ions such as B^{3+} (0.027 nm), Al^{3+} (0.0535 nm) or Ti^{4+} (0.0605 nm) [6–10]. Thus, it would be expected that the insertion of carbon ions (0.016 nm) into the host CdO lattice should significantly improve carrier mobility as well as other CPs. To our knowledge, there have been no reports on the investigation of C-incorporated CdO (CdO–C), although such investigation was conducted on other TCOs such as ZnO [11,12]. The present paper systematically reports the study on the effects of inclusion of C ions on the structural, optical and electrical properties of host CdO thin films, focusing on the improvement to carrier mobility to obtain high optical transparency in the NIR region with low resistivity. It will be seen that insertion of carbon into the host CdO efficiently improved carrier mobility, conductivity and therefore could be used in technical applications based on its TCO properties.

2. Experimental

CdO thin films incorporated with different amounts of carbon element (CdO–C) were deposited on glass substrates by vacuum thermal evaporation technique. The starting materials used were refined sucrose ($C_{12}H_{22}O_{11}$) as a source of carbon impurities and cadmium acetate anhydrate [$Cd(CH_3CO_2)_2$] (from Aldrich Chemical Company). Controlled amounts of starting materials were dissolved in a mixture of ethanol and deionized water (1:1) in a ceramic crucible with continuous

Published online: 09 June 2020

magnetic stirring at room temperature until a colourless liquid was obtained. Then, the temperature was slowly raised to ∼80°C with continuous stirring until a gel was obtained. The crucible was then totally covered with an Al foil and inserted in a closed furnace at a temperature of 500°C for 1 h and then cooled down together to room temperature. The nominal C/Cd mass ratios in the obtained powder samples were 27, 43 and 60%. A part of the created carbon element during the procedure was expected to be free that employed as an evaporation-temperature reducing agent, which reduces the evaporation temperature and obtaining nanograins [13–15]. However, the included carbon in the prepared film samples was measured by using a scanning electron microscope (SEM). Some of the synthesized powder samples were thermally evaporated in a vacuum chamber by using alumina baskets (Midwest Tungsten Service, USA) on clean glass substrates. Then, the as-grown films/glass were annealed in air at 400°C for 1 h keeping the samples inside the closed oven to naturally cool down to room temperature. All the samples were prepared under almost the same conditions. The evaporated masses were controlled with a piezoelectric microbalance crystal sensor (Philips FTM5) fixed close to the substrates. The thicknesses of the prepared films were measured after annealing by using a spectrometer (MP100-M, Mission Peak Optics Inc., USA), to be in the range of 160–240 nm. The weight ratio of C/Cd in each film was measured after deposition by using an SEM (SEM/EDX microscope Zeiss EVO) to be ∼3.5, 4.5 and 5 wt% (referred to as S1, S2 and S3, respectively) in addition to the reference un-doped CdO film (S0 sample) synthesized and prepared by the same procedure. The crystal structures of the prepared films were investigated and analysed by using a Rigaku Ultima-VI X-ray diffractometer (Cu K_α radiation) equipped with a built-in PDXL programme for Rietveld refinement structural analysis. The spectral optical transmittance $T(\lambda)$ and reflectance $R(\lambda)$ were measured at normal incidence in the spectral range (300–1500 nm) with a Shimadzu UV-3600 double beam spectrophotometer. The electrical CPs were measured with a standard van der Pauw technique at room temperature at a magnetic field of ∼1 T.

3. Results and discussion

3.1 *Structural characterization*

Figure 1 displays the X-ray diffraction (XRD) patterns of the prepared pristine and CdO–C films on glass substrates. The standard CdO JCPDS data [16] were used to index Bragg reflections. Therefore, all the investigated CdO–C films were polycrystalline in nature comprising cubic CdO structure of a natural [111] preferred orientation. The inclusion of C ion species in the CdO lattice did not considerably change the degree of natural growth of [111] orientation of the host CdO film, which might be attributed to the occupation of interstitial locations rather than to the occupation of O/Cd

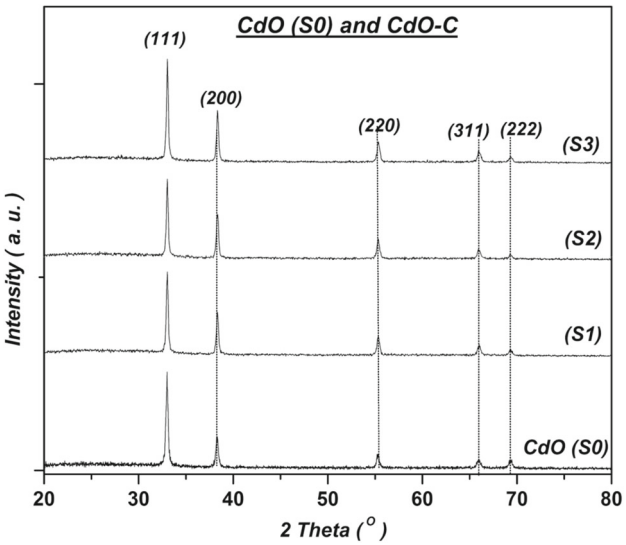

Figure 1. XRD patterns of pristine and CdO–C films deposited on glass substrates.

structural positions. The results of structural analysis are given in table 1. The values of Rietveld statistical refinement parameters (the weighted profile R_{wp}-parameter and the goodness-of-fit S parameter) were satisfactory as the S parameter was <2 indicating an acceptable range [17]. The structural analysis performed by the built-in PDXL programme through the Williamson–Hall method showed that the unit-cell size of the host CdO ($V_{cell} = a^3$) slightly reduced and the structural stress almost remained constant at 0.15%. The average nanocrystallite size increased to ∼44 nm with an increase in C incorporation to 5%. The slight reduction of V_{cell} can be attributed to the small numerical density of created structural vacancies to re-establish unit-cell charge neutrality distorted by the inclusion of small-sized C ion species that occupied interstitial positions.

The substitution for Cd^{2+} ions by dopant C^{4+} ions is unlikely to occur since the difference in the radii (∼83%) could disturb the cubic crystalline structure. Moreover, the possibility of doping of C^{4-} ions (of radius 0.260 nm [18]) for the structural O^{2-} ions would expand the lattice since the difference in the radii is ∼85%. Therefore, the most possible incorporation might be realized by placing the small-sized positive C^{+} ion species (with diverse oxidation numbers) into the interstitial positions in addition to their accumulation on the crystallite and grain boundaries (CBs and GBs). It is expected that the incorporated C^{+} ion species could create structural vacancies, increase the carrier concentration and blue-shift the band gap, which was observed experimentally (sections 3.2 and 3.3).

The increase of carrier concentration N_{el} by ∼2.2−3.4 times with the inclusion of C (section 3.3) suggests that the oxidation states of C ion species were 2+ to 4+ besides some electrically inactive incorporated carbon atoms. Similar results, i.e., the possibility of dopant C to be at higher state

Table 1. Bragg angle (2θ (111)), lattice parameter (a), volume strain (ε_{vs}), Rietveld statistical refinement parameters, CS, structural strain (ε) and texture coefficient ([111]) of the prepared pristine CdO and CdO–C films grown on glass substrates.

Sample	C%	2θ (111)	a (Å)	R_{wp} (%)	S (%)	CS (nm)	ε (%)
CdO	0	32.99	4.702	25.7	1.53	30.4	0.15
S1	3.5	32.99	4.699	13.72	1.12	38.9	0.15
S2	4.5	33.03	4.698	13.47	1.09	38.3	0.13
S3	5.0	33.04	4.696	14.2	1.16	44.1	0.17

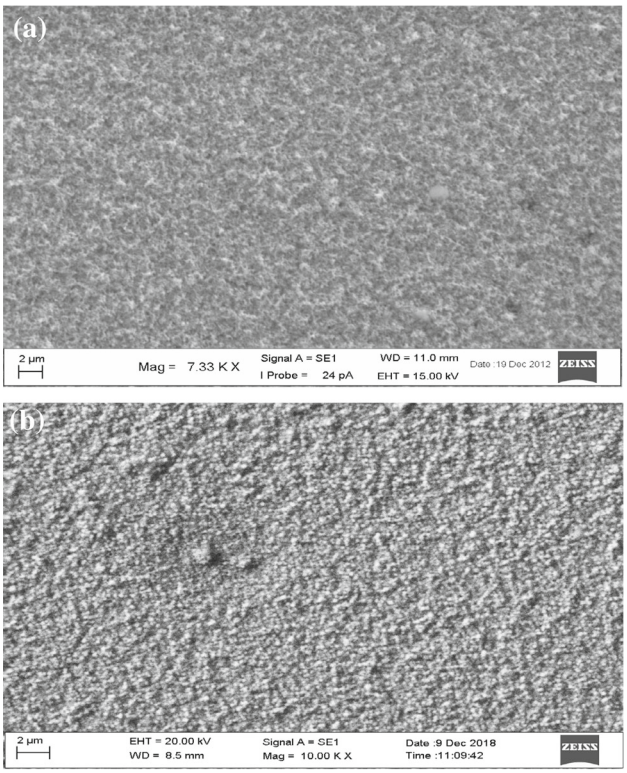

Figure 2. SEM micrographs of (**a**) pristine CdO and (**b**) S3 sample.

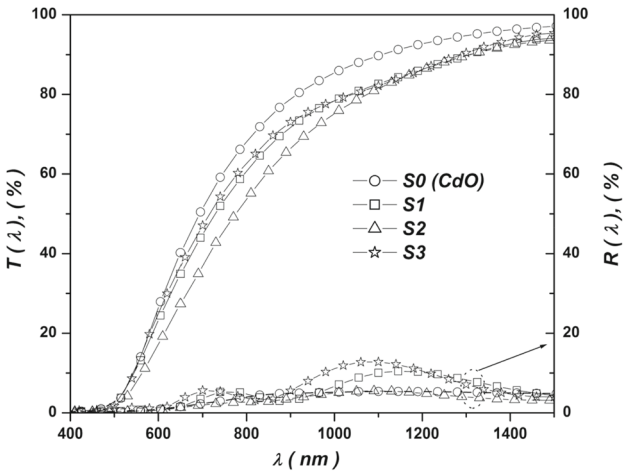

Figure 3. Spectral optical transmittance (T) and reflectance (R) of pristine CdO and CdO–C films deposited on glass substrates.

than the divalent state, were also reported for C-incorporated ZnO films [19].

Figure 2 shows SEM micrographs for (a) pristine CdO and (b) S3 sample. The pure CdO film showed a woolly-shaped element that was converted from C incorporation into almost round grains of size (GS) ∼200−300 nm.

3.2 *Optical characterization*

Figure 3 demonstrates the spectral normal transmittance, $T(\lambda)$ and reflectance, $R(\lambda)$ of the pristine CdO and CdO–C films prepared on corning glass substrates in a spectral region of 400–1500 nm. The transparent region ($T > 50\%$) of pristine CdO is mainly included in the NIR spectral region and slightly shifted deeper into the NIR spectral region with C incorporation. The low-λ side of the spectral $T(\lambda)$ arches shows lower damping character owing to the increase of carbon content (Urbach effect). The normal spectral reflectance, $R(\lambda)$ of the samples shown in figure 2 is almost constant at ∼5%. The spectral absorption coefficient $\alpha(\lambda)$ can be calculated from the experimental $T(\lambda)$ and $R(\lambda)$ by [20]:

$$\alpha(\lambda) = (1/d)\ \ln[(1-R)/T] \tag{1}$$

where d is the film's thickness. The well-known graphical Tauc technique is usually used to compute the direct optical band gap E_g^{op} according to [21]:

$$\alpha(\lambda)E = B_{op}(E - E_g^{op})^{0.5} \tag{2}$$

where B_{op} is the film's constant. The extrapolation of the straight line part of the $(\alpha E)^2$ *vs.* E was plotted for each sample, as shown in figure 4, which gives the value of the optical band gap (table 2) with an estimated accuracy of 0.02 eV. The optical band gap of the undoped CdO (2.29 eV) almost agrees with the previously known values [1,22,23]. The optical band gap of the host CdO has an increasing tendency with an increase in the C incorporation level, as shown in the

inset of figure 6. The blue-shift of the optical band gap E_g^{op} of degenerate semiconductors (such as CdO) is usually attributed to the Moss–Burstein (B–M) effect [24] (next section).

3.3 *Electrical characterization*

The measured CPs of pristine CdO and CdO–C films grown on glass substrates are presented in table 2 and figure 5. The experimental error due to the contact spot size was estimated to be about 5%. The CPs of the pristine CdO film almost agree with the published results for films prepared by different techniques [1,25]. The n-type conductivity measured for pristine CdO and host CdO–C can be attributed to the presence of intrinsic point defects such as oxygen vacancies, Cd vacancies and Cd interstitials. Moreover, the low-resistivity found for the prepared CdO–C films confirms the good quality of inter-crystallite and inter-grain contacts [26]. The results show that an increase in the C% inclusion significantly improved the CPs of the host CdO film. The conductivity and carrier concentration for S0, S1 and S2 increased with C inclusion; similar results were found with the ZnO–C system [11,27]. Moreover, the mobility increased steadily with an increase in C% inclusion for all S0, S1, S2 and S3 films. The increase in the carrier mobility with C% inclusion was expected and mentioned in the 'Introduction' for incorporation of CdO with small-sized ions. However, the present results contradict the previously obtained results on the ZnO–C system, where the mobility decreased by an increase in C% inclusion in the film [11,27].

The ~7.7 times increase in mobility was attained for S3 compared to pristine CdO. Moreover, the C% inclusion in the S3 sample caused an increase in conductivity by ~17 times compared to pristine CdO.

The variations in CPs are presented graphically in figure 4. The electrically measured carrier concentration (N_{el}) increased with the C% inclusion level attaining saturation with S1 and S2, then decreased for the S3 sample. This apparent decrease in electrically measured N_{el} can be attributed to the consequences of accumulation of C-species on CBs and GBs, which supported the surface potential barrier that decreased the electrically measured effective carrier concentration in the S3 sample.

Figure 4 shows a steady decrease in the resistivity of host CdO of all investigated samples. It is interesting to compare with earlier studies on the incorporation of C into ZnO. Pan *et al* [11] found that increasing C% content in ZnO films leads to an increase in conductivity and carrier concentration while decreased the carrier mobility.

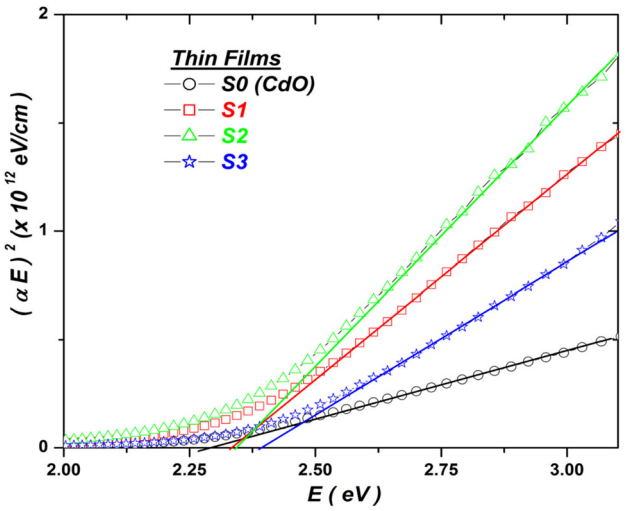

Figure 4. Tauc plot for pristine CdO and CdO–C films.

3.4 *Opto-electrical properties*

The optical and electrical properties of TCO are strongly related to each other. There are two factors that control the measured optical band gap (E_g^{op}): the intrinsic band edge (E_g^{int}) and the B–M electronic contribution (ΔE_g^{BM}) [24]:

$$E_g^{op} = E_g^{int} + \Delta E_g^{BM} = E_g^{int} + S_{BGW} N_{el\text{-}op}^{2/3} \quad (3)$$

The intrinsic direct band gap energy E_g^{int} is due to the electron–lattice interaction that was calculated for CdO by the generalized gradient approximation method was found to be 1.48 eV [28]. The B–M factor contribution is proportional to the optical carrier concentration ($N_{el\text{-}op}$). The calculated coefficient S_{BGW} of the B–M band gap widening for CdO was found to be 1.348×10^{-18} eV m^2 [29]. Thus, the measured optical band gap (E_g^{op}) is correlated with the optical

Table 2. Measured CPs (resistivity (ρ), mobility (μ_{el}) and carrier concentration (N_{el})) and optical band gap (E_g) of the prepared pristine CdO and CdO–C films grown on glass substrates.

Sample	C%	ρ ($\times 10^{-3}$ Ω cm)	μ_{el} (cm^2 V^{-1} s^{-1})	N_{el} ($\times 10^{19}$ cm^{-3})	E_g (eV)
CdO	0	20.1	7.1	4.4	2.29
S1	3.5	2.67	15.7	14.88	2.33
S2	4.5	1.69	25.9	14.2	2.34
S3	5.0	1.19	54.4	9.64	2.39

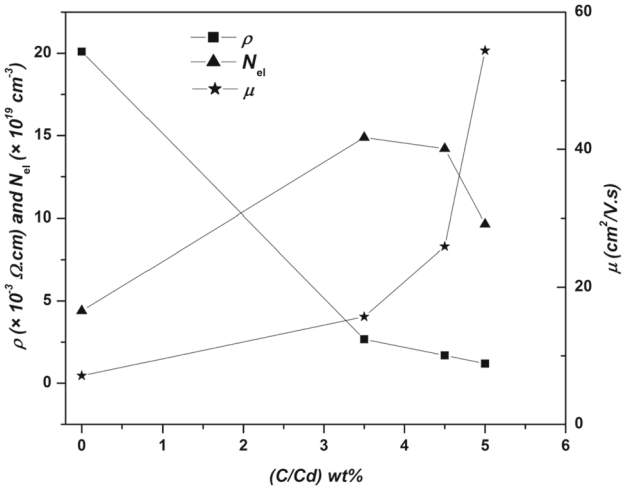

Figure 5. Variation of CPs: resistivity (ρ), mobility (μ_{el}) and carrier concentration (N_{el}) with the C-inclusion level of CdO–C films grown on glass substrates.

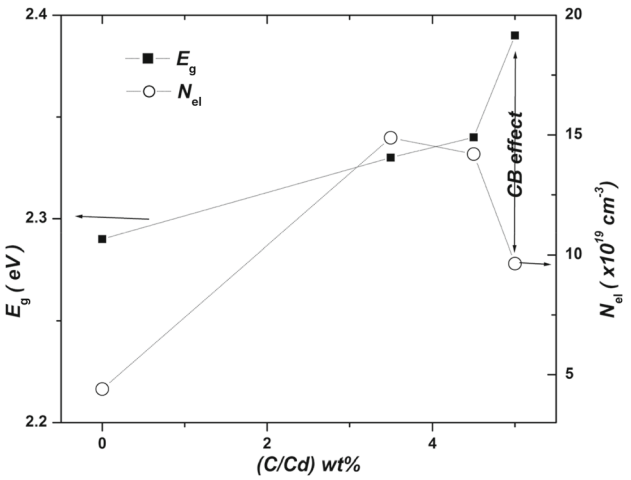

Figure 6. Correlated variation of band gap (E_g) and carrier concentration (N_{el}) with the C-inclusion level of CdO–C films grown on glass substrates.

concentration of carriers of the host CdO as shown in figure 6, which demonstrates the variation in E_g by C% inclusion, plotted together with the dependence on the effective electronic concentration (N_{el}) measured by the electrical method, for comparison and discussion.

The optical band gap (E_g^{op}) was increased by an increase in N_{el} for the S1 sample. However, the optical band gap continued to increase in S2 and S3 samples but with a decrease in electrically measured N_{el}. Such discrepancy could be attributed to the consequence of an increase in the C-species inclusion level, which caused accumulation of C-species on CBs and GBs. The accumulation of C-species on CBs and GBs enhanced the surface potential barrier between the adjacent crystallites that lowered the measured effective carrier concentration (N_{el}) i.e., $N_{el\text{-}op} \geq N_{el}$ for S2 and S3 samples. Therefore, it should be emphasized that the optical concentration of carriers ($N_{el\text{-}op}$) inside the crystallites of S3 sample should be larger than that shown in table 2 (9.64×10^{19} cm^{-3}). Figure 6 demonstrates the CB effect, which stated that the electrically measured carrier concentration (N_{el}) is less than that of optically measured ($N_{el\text{-}op}$) due to the influence of CB surface potential.

The figure of merit (FOM) is defined as T^{10}/R_s, where T is the transmittance of the transparent region and R_s is the sheet resistance [30,31]. The calculated FOMs of the present samples were: $\sim 0.8 \times 10^{-3}$, 3.3×10^{-3}, 5.2×10^{-3} and 1.2×10^{-3} Ω^{-1} for CdO, S1, S2 and S3, respectively. The FOM value of pristine CdO film almost agrees with that obtained in ref. [32]. The FOM increased with lower C% incorporation in the CdO film and reduced with the S3 film.

It should be emphasized that the significance of the quality measure is that FOM needs to utilize the films as transparent conducting electrodes (TCE). In general, the value of FOM depends on the kind of TCO and dopant ions in addition to the details of the preparation procedure [33]. Recently, many researchers have used other types of potential TCEs, such as cracked films [34] and metal mesh networks [35] to obtain better results for potential TCEs. A comparison between the TCEs prepared by different techniques was given in ref. [36].

The experimental measurements show that the growth of crystallite size (CS) supported the value of carrier mobility (table 2). Moreover, the accumulation of amorphous carbon on CBs decreased the resistivity of the host material, which is attributed to low resistivity of amorphous carbon layer that electrically improved the surface contacts between the crystallites.

4. Conclusions

The C-incorporated host CdO thin films have been successfully deposited on glass substrates. Significant effects on the CdO TC properties have been observed. It was concluded that the incorporated small-sized C ion species occupied interstitial locations in the CdO lattice that reduced the size of the host CdO unit cell through the creation of structural lattice vacancies. The inclusion of C ion species led blue-shift of the optical band gap by $\sim$5−7%, which was explained by the B–M effect. The electrical measurements showed that with an increase in the C% inclusion level, the CPs of all investigated host CdO films were much improved. The mobility was significantly increased by $\sim$7.5 times with an increase in C% inclusion of 5%. Therefore, it was confirmed that the host CdO–C film has controllable degenerate TC semiconducting properties that could be used for different practical optoelectronic applications.

Acknowledgements

The author is grateful to Mrs Fatima H Qabeel from the SEM Laboratory/Central Labs/College of Science (UOB).

References

[1] Zhao Z, Morel D L and Ferekides C S 2002 *Thin Solid Films* **413** 203
[2] Robertson J and Falabretti B 2011 in *Handbook of transparent conductors* D Ginley, H Hosono and DC Paine (eds) (Springer Science + Business Media, LLC) p 27
[3] Chandiramouli R and Jeyaprakash B G 2013 *Solid State Sci.* **16** 102
[4] Carballeda-Galicia D M, Castanedo-Perez R, Jimenez-Sandoval O, Jimenez-Sandoval S, Torres-Delgado G and Zuniga-Romero C I 2000 *Thin Solid Films* **371** 105
[5] Shannon R D 1976 *Acta Crystallogr. Sect. Found. Crystallogr. A* **32** 751
[6] Dakhel A A 2011 *J. Mater. Sci.* **46** 6925
[7] Gupta R K, Ghosh K, Patel R, Mishra S R and Kahol P K 2009 *Curr. Appl. Phys.* **9** 673
[8] Saha B, Das S and Chattopadhyay K K 2007 *Sol. Energy Mater. Sol. Cells* **91** 1692
[9] Murali K R, Kalaivanan A, Perumal S and Neelakanda Pillai N 2010 *J. Alloy Compds.* **503** 350
[10] Gupta R K, Ghosh K, Patel R and Kahol P K 2009 *Appl. Surf. Sci.* **255** 6252
[11] Pan H, Yi J B, Shen L, Wu R Q, Yang J H and Lin J Y *et al* 2007 *Phys. Rev. Lett.* **99** 127201
[12] Subramanian M, Akaike Y, Hayashi Y, Tanemura M, Ebisu H and Ping D L S 2012 *Phys. Status Solidi B* **249** 1254
[13] Lv H, Sang D D, Li H D, Du X B, Li D M and Zou G T 2010 *Nanoscale Res. Lett.* **5** 620
[14] Xu C X, Sun X W, Dong Z L and Yu M B 2004 *Appl. Phys. Lett.* **85** 3878
[15] Yao B D, Chan Y F and Wang N 2002 *Appl. Phys. Lett.* **81** 757
[16] Powder Diffraction File, Joint Committee for Powder Diffraction Studies (JCPDS) file no. 05-0640
[17] McCusker L B, Von Dreele R B, Cox D E, Louer D and Scardi P 1999 *J. Appl. Crystallogr.* **32** 36
[18] Zhou S, Xu Q, Potzger K, Talut G, Grötzschel R, Fassbender J *et al* 2008 *Appl. Phys. Lett.* **93** 232507
[19] Akbar S 2017 *Defect ferromagnetism in ZnO and SnO_2 induced by non-magnetic dopants* (Dissertation, University of Groningen north-west Germany (UGNWG)) p 41
[20] Hong W Q 1989 *J. Phys. D: Appl. Phys.* **22** 1384
[21] Tauc J and Abelesn F (eds) 1969 *Optical properties of solids* (New York: North-Holland Publishing Co)
[22] Kawamura K, Maekawa K, Yanagi H, Hirano M and Hosono H 2003 *Thin Solid Films* **445** 182
[23] Naser G Y, Raja W N, Faris A S, Rahem Z J, Salih M A and Ahmed A H 2013 *Energy Procedia* **36** 42
[24] Pankove J I 1975 *Optical processes in semiconductors* (NY: Dover Publications) p 36
[25] Anitha M, Tamilnayagam V, Anitha N, Amalraj L and Raj S G 2017 *J. Mater. Sci.: Mater. Electron.* **28** 17297
[26] Zhange S B, Wei S-H and Zunger A 2001 *Phys. Rev. B* **63** 075205
[27] Akbar S, Hasanain S K, Abbas M, Ozcan S, Ali B and Shah S I 2011 *Solid State Commun.* **151** 17
[28] Zhang F C, Cui H W, Ruan X X and Zhang W H 2014 *J. Chem. Pharm. Res.* **6** 1658
[29] Dakhel A A and Hamad H 2013 *J. Solid State Chem.* **208** 14
[30] Velusamy P, Ramesh Babu R, Ramamurthi K, Dahlem M S and Elangovan E 2015 *RSC Adv.* **5** 102741
[31] Hassanien A E, Hashem H M, Kamel G, Soltan S, Moustafa A M, Hammam M *et al* 2016 *Int. J. Thin Films Sci. Technol.* **5** 55
[32] Velusamy P, Ramesh Babu R, Ramamurthi K, Elangovan E, Viegas J, Dahlem M S *et al* 2016 *Ceram. Int.* **42** 12675
[33] Lee D, Lee H, Ahn Y, Jeong Y, Lee D-Y and Lee Y 2013 *Nanoscale* **5** 7750
[34] Mondal I, Kumar A, Rao K D M and Kulkarni G U 2018 *J. Phys. Chem. Solids* **118** 232
[35] Singh A K, Kiruthika S, Mondal I and Kulkarni G U 2017 *J. Mater. Chem. C* **5** 5917
[36] Gupta R, Rao K D M, Kiruthika S and Kulkarni G U 2013 *ACS Appl. Mater. Interfaces* **5** 730